Formation of Ni-graphite intercalation compounds on SiC

K. Robbie,* S. T. Jemander, N. Lin, C. Hallin, R. Erlandsson, G. V. Hansson, and L. D. Madsen
Department of Physics, Linköping University, S-581 83, Linköping, Sweden
(Received 19 March 2001; published 18 September 2001)

We report the observation, by scanning tunneling microscopy (STM), scanning electron microscopy (SEM), Auger electron spectroscopy (AES), and atomic force microscopy (AFM), of a graphite intercalation compound (GIC) formed by a new mechanism. Ni films with a nominal thickness of 2.5 monolayers were sputter deposited onto single-crystal 6H-SiC (0001) substrates heated to 600 °C in an ultrahigh-vacuum STM system. When the substrates are annealed to 800–1000 °C, the formation of islands is observed by STM. The islands were ~0.3 μm in diameter, ~30 nm high, and separated by 5 μm from each other, with an exceptionally flat top with a peculiar ''stitched'' surface structure. A second type of island, ~1.5 μm in diameter, ~10 nm high, and separated by ~10 μm from each other, was observed by AFM and SEM. Microspot AES showed that the first islands are composed of Ni and C, while the second islands are composed of Ni, C, and Si. AES line shape studies showed that the C in both types of islands is graphitically bound. AES line shape analysis of the carbon in the substrate (SiC) verified carbidic binding. From comparisons to the literature, we believe that the first islands are a new type of GIC. An indexing of Ni on the top graphite sheets is presented for each anneal temperature.

DOI: 10.1103/PhysRevB.64.155401 PACS number(s): 81.05.Tp, 81.05.Zx, 68.37.Ef, 81.10.Jt

I. INTRODUCTION

Graphite intercalation compounds (GICs) form when a chemical species penetrates (intercalates) into the galleries between sheets of graphite.[1] The intercalating species can be elemental (Li, Na, K, Rb, etc.), molecular ($NiCl_2$, MoF_6, $CuCl_2$, etc.), or binary or ternary combinations ($KHgC_4$, etc.). GICs have been studied extensively both experimentally and theoretically[2] with a wide range of techniques, and have shown a remarkable range of physical properties. Many GICs are superconducting even though neither the intercalant nor graphite are superconducting alone,[1] and the magnetic, catalytic, and other properties of GICs differ significantly from those of the intercalating material in bulk.[3,4,5] The ability to alter the properties of graphite, and of the intercalant material, by the formation of GICs makes them technologically interesting for a range of applications including, for example, magnetic storage, hard coatings, and optical materials. Also, quasi-two-dimensionality or even one-dimensionality makes them scientifically interesting as model systems for the study of solid-state physics and chemistry.

There has been significant scientific investigation of GIC formation in the last 20 years, resulting in the discovery of more than 100 phases, fabricated with a variety of synthesis methods.[6] GICs are most commonly fabricated by liquid or gas phase reaction of the intercalation species with a preexisting graphite host, typically highly oriented pyrolytic graphite (HOPG), at elevated temperature (~500 °C) for extended periods of time (~20 days). Modifications of the standard process can involve, for example, alternate intercalant chemistries (halogens, halides, hydroxides, metal oxides, etc.) and/or high pressure. Because most GICs are formed by diffusion of the intercalant species between preexisting layers of graphite, kinetic limitations preclude the fabrication of GICs with a large number of potentially interesting intercalants, e.g., most transition metals and semiconductors. While some of these materials can be carried into the graphite host as a molecular species (e.g., $NiCl_2$) and then chemically reduced, this process always leaves a significant amount of the carrier species within the GIC (e.g., $NiCl_{2.13}C_{11.3}$),[3,7] and can lead to the formation of clusters of intercalant atoms.[8] Recently, Grigorian *et al.*[9] reported a chemical vapor deposition (CVD) technique where graphite is grown from a hydrocarbon vapor in the presence of the desired intercalation species vapor (Se in this case). Their technique is promising and may lead to GICs with previously unobtainable intercalants. Interestingly, in relation to this work, their technique employs the ''catalytic action of a transition metal (e.g., Ni) substrate'' to encourage graphite growth. Finally, two reports in the literature exist of a GIC fabricated using vacuum thin-film deposition techniques. In one, a La-GIC is described, formed by annealing thin films of La, which were vacuum evaporated onto HOPG.[10] In the second, ultraviolet photoemission spectroscopy and high-resolution electron energy-loss spectroscopy analysis was used to study the interaction of Cs evaporated onto a highly graphitized SiC surface.[11] Observed changes in work function and electron energy-loss spectra suggest initial intercalation of Cs into the uppermost graphite layers before the formation of a metallic surface layer.

When GICs have been studied by scanning tunneling microscopy (STM), a large number of interesting structures were observed. The lattice formed by the intercalant atoms or molecules disrupts the normal physical and electronic structure of the host graphite, resulting in various observed effects. Anselmetti *et al.*,[12,13,14] Lang *et al.*,[15,16] and Miyake *et al.*[17] observed (2×2), $(\sqrt{3}\times4)$, $(\sqrt{3}\times\sqrt{13})$, and $(\sqrt{3}\times\sqrt{3})$ hexagonal and nonhexagonal superlattice structures, including one-dimensional (1D) phases which appear to be very similar to those presented in this work. These observed structures are explained as arising from the ordering of the intercalating metal atoms situated either on top of, or within the first gallery below, the topmost graphite sheet. Olk

et al.[18] showed that the $CuCl_2$ intercalant superstructure is imaged when the STM tip is positively biased with respect to the sample and that the overlying topmost graphite layer is imaged when the STM tip is negatively biased. One-dimensional structures were attributed to either charge-density-wave (CDW) effects[15–17] or to depletion of alkali metal from subsurface galleries of the GIC.[13,14]

A recent theoretical treatment of graphite intercalation[2] illucidates some of the key concepts of the work presented in this paper. Taking a graphite lattice with 6 layers of 220 atoms each, and using molecular dynamics simulation, ordering of initially random intercalant atoms into one-dimensional chains and two-dimensional clusters is observed over time. An empirical potential function is employed that treats both the sp^2 bonding between the carbon atoms in the graphite layers and the van der Waals and repulsive forces that hold the graphite layers together, yet separated. Tight-binding molecular dynamics simulations show initially random intercalant atoms (carbon in this case) diffusing and forming 1D and 2D ordered clusters. This demonstrates the theoretical feasibility of intercalant compounds similar to that seen in the present paper, without an alkali metal or metal compound (chloride, bromide, etc.) intercalant. It also presents a discussion of a potential function between the graphite sheets that leads to the formation of ordered layers, as is observed in our work.

Because of the importance of Ni as a catalyst for methanation of CO ($CO+3H_2=CH_4+H_2O$), the Ni-C and Ni-graphite system has been extensively studied,[19–24] and the growth of graphite overlayers on Ni is well described, including with STM analysis. No indication of the formation of Ni-GICs was found in this literature, however. We believe this is because methenation occurs at lower temperatures than those used in this work. No reports were found that employed the temperature regime used in this study (800–1000 °C). Investigation of the metallurgical literature also yielded no mention of Ni-GICs. From these studies, there are few Ni-C binary alloys: a low-temperature nickel carbide metastable phase, Ni_3C, exists, but decomposes above 400 °C. Above 400 °C, the highest observed C content is about 7 at. % (at 1300 °C) in solid solution in Ni.[25]

In this work, thin layers of Ni were sputter deposited onto single-crystal SiC substrates at elevated temperatures (600 °C). After annealing to higher temperatures (800–1000 °C), the formation of small islands of Ni-GICs was observed. To the best of our knowledge, this is the first report of a pure transition metal GIC.[26,27,5,7,3]

II. EXPERIMENT

Ni films of varying thicknesses were sputter deposited, within an ultrahigh-vacuum (UHV) STM system, onto single-crystal 6H-SiC (0001) substrates heated to 600 °C. The substrates were then heated to 1000 °C with STM imaging performed at three temperature steps. *Ex situ* analysis included microspot Auger electron spectroscopy (AES) and AES line shape studies, scanning electron microscopy (SEM), and atomic force microscopy (AFM).

The UHV-STM instrument used in this work is described in detail in Ref. 28. It routinely achieves atomic resolution with its high-stability scanning tunneling microscope within a UHV chamber [with a base pressure less than 5×10^{-11} Torr (7×10^{-9} Pa)]. Attached to the main chamber is a sample preparation chamber with a 2.5-cm-diam sputter gun and a base pressure of 5×10^{-10} Torr (7×10^{-8} Pa). Substrates are $\sim 8\times10\,mm^2$ in size with a thickness of 300 μm that are clamped into Ta or Mo holders. Heating is performed resistively with a large current passing through the substrate. The STM piezoelectric scanners were calibrated by scanning the Si(111) 7×7 and SiC(0001) $\sqrt{3}\times\sqrt{3}$ surfaces. Scanning tips were prepared by electrochemically etching tungsten wires.

The substrates used for this study were single-crystal 6H-SiC (0001) pieces cleaved from *n*-type substrates from Cree Research Inc.[29] They were nominally on axis (specified less than 0.5° off-cut) and measured by x-ray diffraction to be 0.16° off. The wafer was cleaved into pieces to fit the STM sample holder. The pieces were then cleaned with the following steps: $NH_3+H_2O_2+H_2O$ (1:1:5) near boiling for 5 min; rinse in de-ionized (DI) H_2O; $HCl+H_2O_2+H_2O$ (1:1:6) near boiling for 5 min; rinse in DI, $HF+H_2O$ (1:5) for 1 min; N_2 drying. They were then hydrogen etched in a hotwall CVD reactor at ~1500 °C for 30 min to remove about 200 nm of SiC, thereby eliminating polishing scratches and resulting in large atomically flat terraces separated by single unit-cell steps.[30–32] The substrates were then stored under high vacuum until they were loaded into the STM chamber. Once within the chamber, they were heated to 950 °C for 2 min to remove any surface impurities. They were cooled and imaged both with low-energy electron diffraction (LEED) and STM, confirming a $\sqrt{3}\times\sqrt{3}R30°$ surface of clean SiC. A filled-state STM image of the cleaned, H_2 etched, and heated surface is shown in Fig. 1(a). Four large terraces, ~150 nm wide, are observed, separated by single 6H-SiC unit-cell steps of 1.5 nm. Higher-resolution scans (not shown) reveal that the terraces exhibit the $\sqrt{3}\times\sqrt{3}R30°$ reconstruction, with some surface defects. These observations are in agreement with previous studies of H_2-etched 6H-SiC.[30–32]

Ni was deposited onto the substrates by dc magnetron sputtering at 2 W in 5 mTorr (670 mPa) of Ar gas. The deposition rate was calibrated periodically by measuring the thickness, by glancing angle x-ray diffraction, of test films deposited onto unheated oxidized Si substrates. While a variety of film deposition temperatures were used in the larger study of nickel-silicide formation of which this paper is one part, all samples described herein were heated to 600 °C during deposition and were coated with Ni to a nominal thickness of 0.4 nm [approximately 2.5 monolayers (ML)]. The substrate temperature was measured with an infrared pyrometer [Minolta Co. (Ref. 33)] with an emissivity set to 0.83, looking through a glass viewport into the vacuum system. Temperature variation across the sample was ~30 °C when a substrate was heated to 1000 °C, with a large area of uniform temperature in the center bordered by cooler areas toward the Ta/Mo holder clips. After deposition, each sample was cooled and imaged in the STM. Heat treatments were made at 800, 900, and 1000 °C for 2 min followed by cooling at

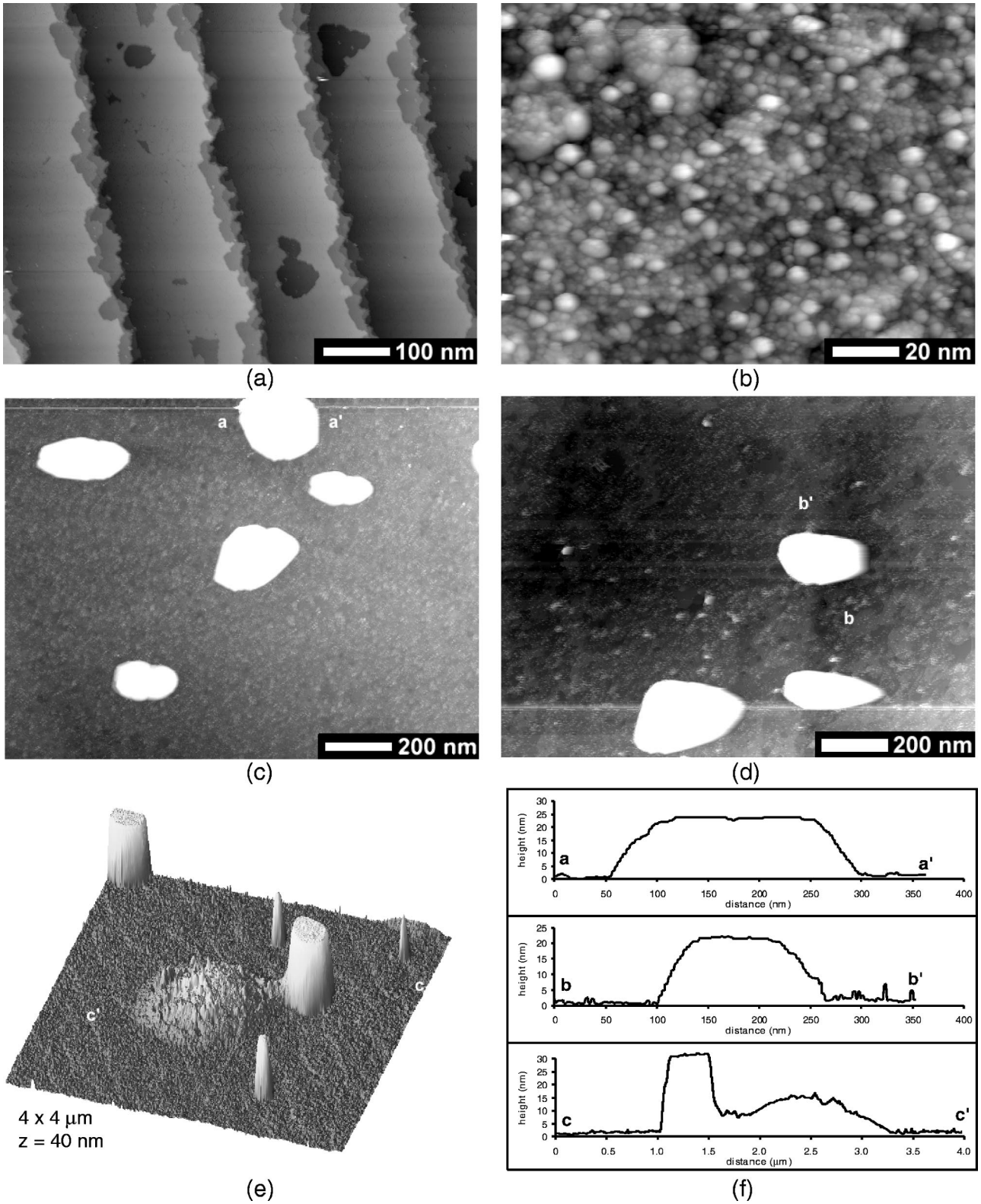

FIG. 1. (a) STM image of the clean SiC substrate after H_2 etching ($V_T = 2.73$ V, 100 pA), (b) after deposition of 2.5 ML of Ni at 600 °C ($V_T = 3.0$ V, 162 pA), (c) after anneal to 800 °C ($V_T = 2.45$ V, 180 pA), (d) after anneal to 900 °C ($V_T = 2.18$ V, 200 pA), (e) 4×4 μm^2 AFM image, with 40 nm vertical scale, after anneal to 1000 °C, and (f) line profile cross sections indicated in images (c)–(e).

approximately 100 °C/s when the resistive heating was turned off.

After the final STM imaging, the samples were removed from the STM chamber for *ex situ* SEM, AES, and AFM analyses. SEM and AES analyses were performed in a VG Scientific[34] Microlab 310-F system which has a field-emission electron gun and is capable of high-spatial-resolution AES. The electron beam energy used was 10 kV and the system base pressure was below 1×10^{-9} Torr (1.3×10^{-7} Pa). SEM analysis was performed with secondary-electron detection. AES scans of a large range of the electron energy spectrum were performed on the two types of observed islands, and on the substrate, to determine chemical composition and state. Spatial resolution was limited due to a slight specimen drift, and spots smaller than 200 nm square could not be analyzed reliably. High-energy-resolution line-shape analysis was performed on the carbon *KVV* Auger line at 270 eV to determine bonding type (graphitic or carbidic). AFM imaging was also performed on the samples after removal from the STM chamber. A Digital Instruments[35] Nanoscope IIIa microscope was used in tapping mode, with a silicon cantilever tip. Post acquisition processing of the STM, AFM, and SEM images presented was performed to increase contrast and clarity when needed.[36] Line profiles presented were acquired before any image processing and represent raw data.

III. ANALYSIS

The clean SiC surface before any Ni deposition is shown in a filled-state STM image in Fig. 1(a). Four 6H-SiC single-unit-cell steps of 1.5 nm cross the image. The $\sqrt{3}\times\sqrt{3}R30°$ reconstruction covered most of the surface, as expected for a clean SiC surface heated to 950 °C.[37,38] No evidence of 6×6 or 5×5 reconstructions were observed, indicative of the onset of surface graphitization of SiC surfaces heated above 1050 °C,[37,38] supporting the accuracy of the temperature measurements performed with the infrared pyrometer. At the annealing temperature used (950 °C), the SiC surface is expected to be at its cleanest, with no hydrocarbon or oxygen contamination. At higher temperatures, Si depletion begins and eventually (above 1200 °C) graphite forms on the surface.[38]

After depositing 2.5 ML of Ni at 600 °C, the surface roughened, as shown in the STM image of Fig. 1(b). A surface, typical of low-temperature metal deposition,[39] appeared with regions ~5 nm in diameter. The composition of this surface is not known, but Madsen *et al.*[39] showed that Ni deposited at lower temperatures will react with SiC to form a nickel silicide ($Ni_{31}Si_{12}$) when annealed to 600 °C. The fate of the carbon has not been adequately resolved and remains an open problem for the reliability of nickel silicide contacts to SiC electronic devices.[40] Many larger scans of up to 2.5 μm square were conducted on the as-deposited film, and no other features were observed.

When the sample was heated to 800 °C for 2 min, the formation of islands was observed by STM. Figure 1(c) shows a filled-state STM image of a number of these islands. The islands are typically ~100–250 nm in diameter and 20–30 nm high, with flat tops and sharp sidewalls [line profile a-a' in Fig. 1(f)]. They appear to be randomly distributed across the substrate without preferential location on step edges or terraces. After heating to 900 °C, similar islands were observed, Fig. 1(d), and the line profile b-b' in Fig. 1(f) has similar dimensions.

When samples heated to 1000 °C were imaged by STM, islands similar to those observed at 800 °C and 900 °C were observed; however, imaging by AFM and SEM revealed two distinct island types. As all samples were annealed to 1000 °C before removal from the STM chamber, AFM imaging of 800 °C and 900 °C heated samples was not possible. The first type of island (type 1) corresponds to the islands observed by STM. Type-2 islands are larger in diameter and shorter than type-1 islands. Figure 1(e) is an AFM scan showing both types of islands, and the marked line profile c-c' is shown in Fig. 1(f). The large-diameter low island in the center is a type-2 island, and the two tall islands with flat tops are type 1; the three smaller-diameter tall islands are possibly type-1 islands in earlier stages of formation. After the 1000 °C anneal, the type-1 islands have increased in size to ~500 nm in diameter and to ~30 nm in height. Type-2 islands are typically ~1.5 μm in diameter and ~10 nm high, and while type-2 islands were not observed by STM, it is likely that they were missed since the largest scan possible with the STM is a $2.5\times2.5\ \mu m^2$ region, and type-2 islands have typically ~10 μm separation.

A larger area AFM scan showing both types of islands clearly is shown in Fig. 2(a). There are ~100 type-1 and 25 type-2 islands in this image, giving densities of ~0.13 and ~0.03 islands per μm^2, respectively. The height scaling of Fig. 2(a) has been chosen to demonstrate two features: (i) the steps in the SiC surface which vary somewhat in orientation, as explained by Ramachandran *et al.*[32] and (ii) the existence of large-diameter depressions around type-2 islands. These depressions are typically ~3–4 μm in diameter, ~1–2 nm deep, and are not necessarily centered on the type-2 islands, which they contain. Depressions were observed around most, but not all, type-2 islands. (Type-1 islands were never observed to be surrounded by depressions.) The depressions are seen more clearly in a perspective view AFM image in Fig. 2(b) where there are eight type-2 islands, three with clear depressions, and 33 type-1 islands. The relationship between the two types of islands was investigated extensively with AFM without discovery of a clear correlation. Most islands, of both types, appeared to exist independently of any other island. There were some instances, however, when type-1 and type-2 islands coexisted. The large type-2 island in Fig. 2(c) appears to have three type-1 islands in contact with it or growing from it. Another arrangement observed was that of a type-1 island and a type-2 island in close proximity with a small ''neck'' of material joining them [see Fig. 1(e)]. The two type-2 islands on the right side of Fig. 2(b) both have this geometry. It must be stressed, however, that this is a rarity. Most type-2 islands imaged with AFM had smooth tops and there was no indication of type-1 islands nearby.

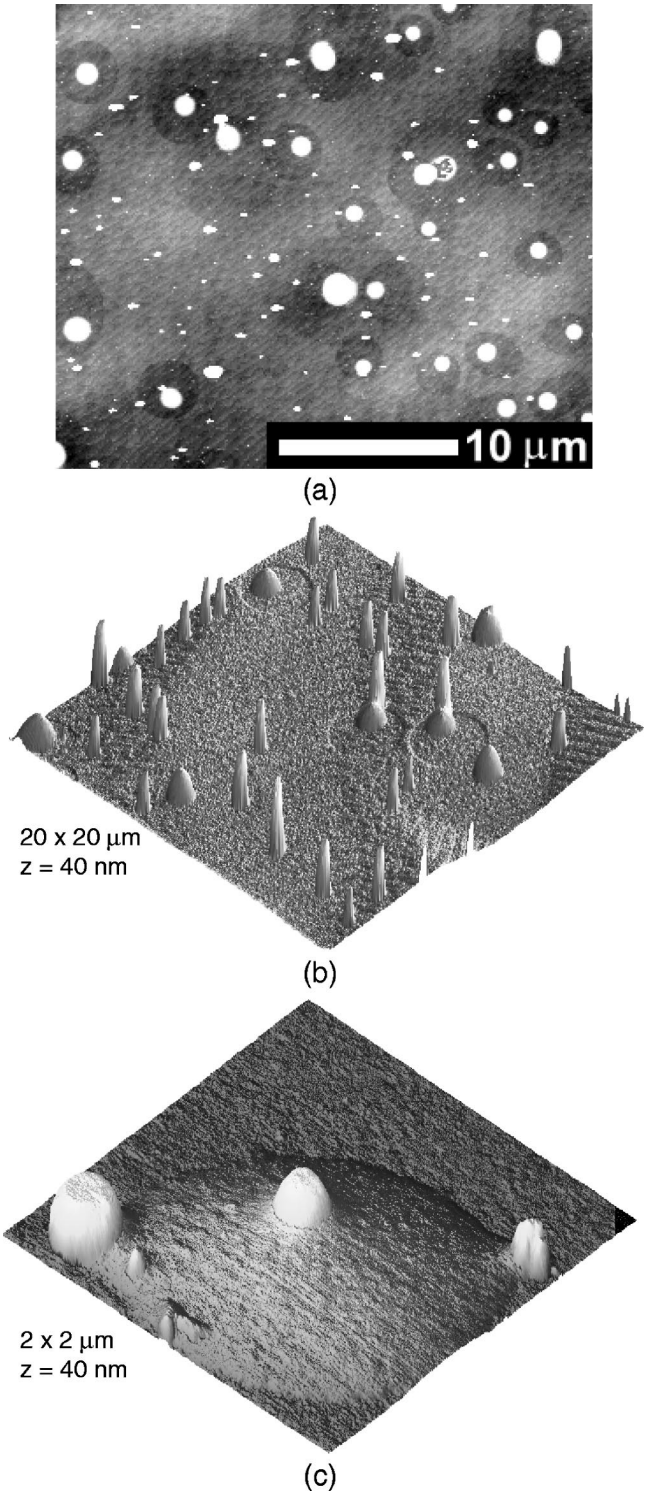

FIG. 2. (a) $26\times30\,\mu m^2$ AFM scan after anneal to 1000 °C showing two island types, (b) $20\times20\,\mu m^2$ AFM perspective view, with 40 nm vertical scale, showing islands and depressions, and (c) $2\times2\,\mu m^2$ AFM perspective view, with 40 nm vertical scale, showing both island types.

The composition of these islands observed by AFM, SEM, and STM was determined using microspot AES analysis. Figure 3(a) is a SEM image showing the two island types as well as the depressions surrounding type-2 islands. Type-1 islands appear as bright spots, while type-2 islands appear dark. While this is the opposite of the AFM images of Fig. 2, it is unsurprising as AFM and SEM measure different things (topographical height and secondary electron yield, respectively). The depressions around the type-2 islands are imaged by SEM as a light area around the dark islands. AES spectra were taken on many islands and substrate locations and found to be consistent, and representative spectra are shown in Fig. 3(b), corresponding to the marked locations on the SEM image. Each spectra is composed of two parts: a direct mode showing a kinetic energy spectrum from 100 to 2000 eV and a first-derivative mode showing a high-energy-resolution section of the spectrum around the carbon *KVV* peak at 270 eV. From these spectra we deduce the following: type-1 islands are composed of primarily C and Ni with only a trace of Si; type-2 islands contain C, Ni, and Si; and the area without islands contains C and Si with only a trace of Ni. Additionally, type-1 islands show significantly more contamination with O than the other two areas. The size of the type-1 islands was at the limit of the spacial resolution of the AES system, and therefore some of the Si and C signal may have come from the substrate.

As the height difference of the depressions surrounding type-2 islands was on the order of 1 nm, it is somewhat surprising that there was significant contrast observed by SEM [Fig. 3(a)]. Strong variation in secondary electron yield usually arises from variation in conduction electron density;[41] however, AES analysis, performed inside and outside the depressions surrounding type-2 islands, revealed no appreciable difference, neither in composition nor in the state of the carbon, silicon, or nickel bonding. As the secondary-electron detector used for SEM imaging samples primarily very-low-energy electrons ($<$10 eV, which come from very near the surface, $<$1 nm),[41] and AES spectra were taken at higher energies ($>$250 eV, which can come from further into the bulk, $\sim$3 nm),[41] this suggests that a compositional difference may exist in a very thin layer on the surface. As the SiC substrate has a low conductance (and a low conduction electron density), while nickel silicides have a relatively high conductance (and a high conduction electron density), the existence of a thin ($<$1 nm) nickel silicide layer outside the depressions, and its absence inside, could explain the observed secondary electron contrast, while allowing for the lack of variation in composition observed by AES. This is consistent with the thickness of the Ni film, 0.4 nm, initially deposited on the SiC substrate. Future AES analysis of low-energy Auger peaks might be helpful in resolving this.

The small derivative spectra displayed above the carbon AES peak in Fig. 3(b) show the difference in the bonding of carbon in the islands compared to that in the SiC substrate. No difference was observed in lineshape between type-1 and type-2 islands, but there was a marked difference between the lineshape observed from the carbon in the islands versus the carbon in the substrate. Figure 4 shows this in more detail. The spectra are first-derivative spectra centered on the carbon *KVV* peak at 270 eV. The lineshape is dependent on the local chemical environment (bonding) of the carbon from which the Auger electrons originate. The upper spectra in

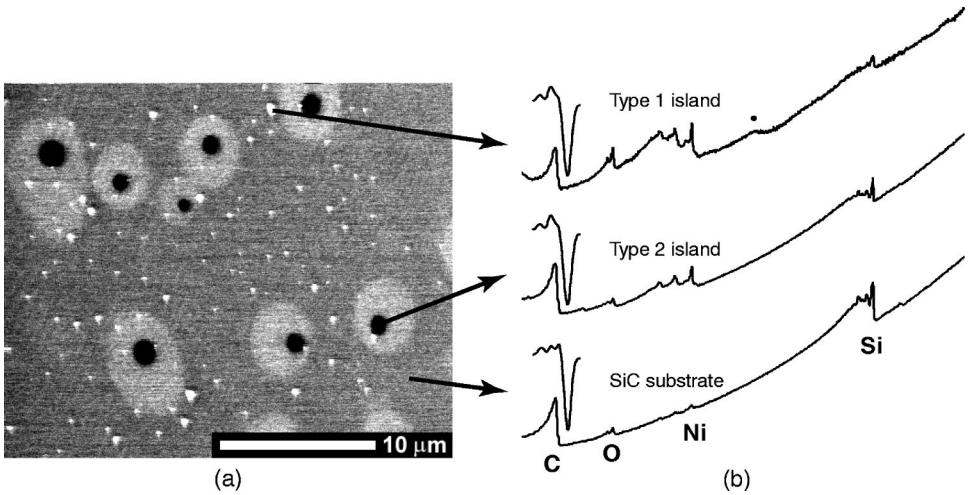

FIG. 3. (a) SEM image showing both island types and depressions and (b) microspot AES spectra of both island types and of uncoated substrate. Insets above the carbon peaks are first-derivative high energy-resolution scans of the carbon *KVV* peak at 270 eV. The small peak (marked·) on the top spectrum (type-1 island), between Ni and Si in energy, arose when the electron beam was moved slightly, during the AES scan, to compensate for drift.

Figs. 4(a) and 4(b) are from Amoddeo *et al.*[42] and correspond to nickel carbide and graphite, respectively; the lower spectra were measured beside the islands (a), and on the islands (b), respectively. Because of the high spatial resolution required to image the islands, small apertures were needed in the electron column, resulting in a low beam current and making it difficult to obtain high energy resolution. As a result, our measured spectra are not as detailed as those of Amoddeo *et al*. However, it is clear that the carbon bonding within the islands is ''graphitic'' as opposed to that in the silicon carbide substrate where it is ''carbidic.'' While inert gas ion sputtered depth profiles might seem a logical analysis technique to employ to further the analysis of these islands, ion-induced carbide formation occurs quite readily in many carbon-metal systems,[43] making this analysis problematic.

In summary, type-2 islands are composed of Ni, graphitically bound C, and Si, are typically ~1.5 μm in diameter and ~10 nm high, and are surrounded by noncentered depressions 3–4 μm in diameter and ~1 nm deep. As these islands were not observed within the STM system, the temperature at which they formed is unknown—all samples were annealed to 1000 °C before removal from the STM. So what mechanism could form such islands? What mechanism could result in a depression surrounding an island? Within the accuracy of the AFM measurements, the volume of the type-2 islands is approximately equal to the volume of the surrounding depressions, suggesting that the depression may have formed when existing material melted to create a liquid droplet and became the type-2 island when quenched. Nickel on SiC usually forms nickel silicides when annealed to high temperatures, Ni_2Si above 770 °C,[39] but because we lack x-ray diffraction or other analysis results to determine the silicide phase and as the phase formation may differ because the Ni was deposited onto heated substrates, it is not know with certainty if Ni_2Si was the phase formed. Carbon, which is known to be liberated by the silicide formation process,[39] may exist as disordered, but graphitically bound, precipitates throughout the nickel silicide layer and the type-2 islands. Studies of the ternary Ni-Si-C system in bulk show, in an isothermal section at 1150 °C, a liquid phase which exists over a large range of composition from about $Ni_{0.45}Si_{0.55}$ to $Ni_{0.65}Si_{0.35}$ with C content up to about 10%.[44,45] This liquid phase coexists with solid SiC and Ni_2Si. There are a large number of nickel silicides seen in bulk[25] with a large range of melting temperatures. Ni-rich phases Ni_3Si, $Ni_{31}Si_{12}$, and Ni_2Si have high melting temperatures 1170, 1242, and 1306 °C, respectively, but both NiSi and $NiSi_2$ have melting temperatures of ~965 °C, similar to that required to support the hypothesis that type-2 islands are formed by the melting of silicide regions. Interestingly, only Ni-rich phases were observed in the detailed synchrotron XRD study with *in situ* annealing, performed by Madsen *et al.*,[39] of nickel silicide formation for Ni initially deposited at low temperatures onto SiC.

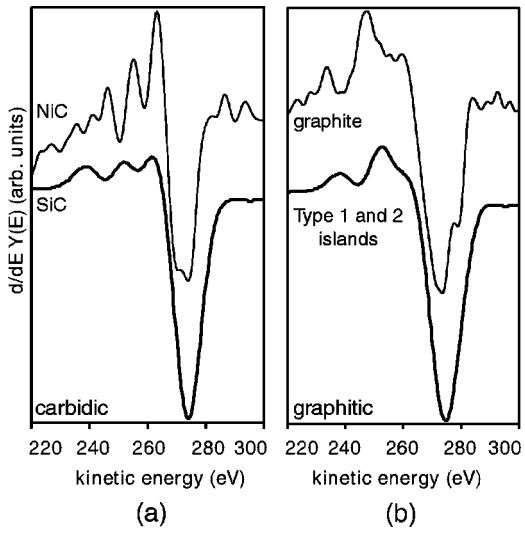

FIG. 4. Auger lineshapes of carbon *KVV* peak at 270 eV. (a) ''Carbidic'' carbon from nickel carbide (top) and SiC substrate between islands (bottom) and (b) ''graphitic'' carbon from graphite overlayer on nickel (top) and type-1 and type-2 islands (bottom).

Type-1 islands, however, were extensively studied by STM in UHV. The tops of the islands were found to be atomically flat with height variations of <0.1 nm, and the sidewalls were very steep. When observing sharp features with STM or AFM, the observed steepness is always limited by the sharpness of the STM or AFM tip. The sharpest ob-

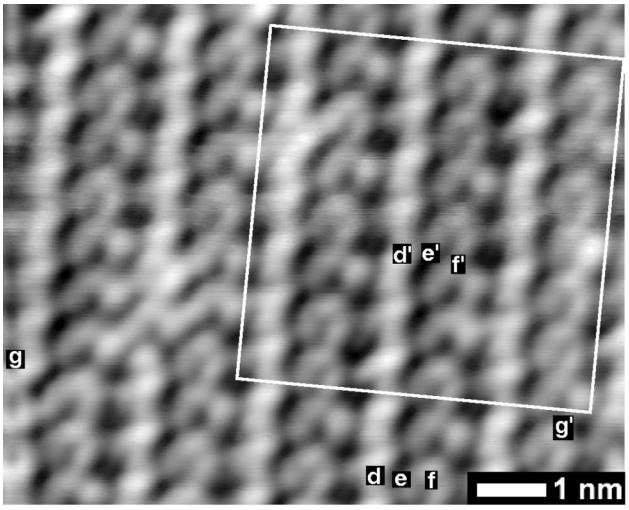

(a)

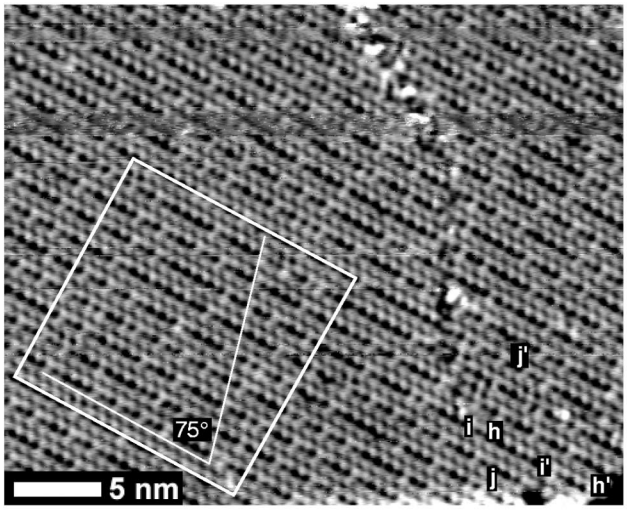

(b)

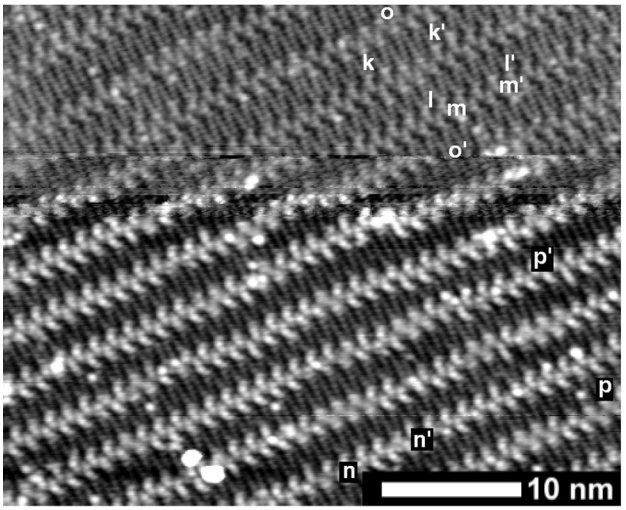

(c)

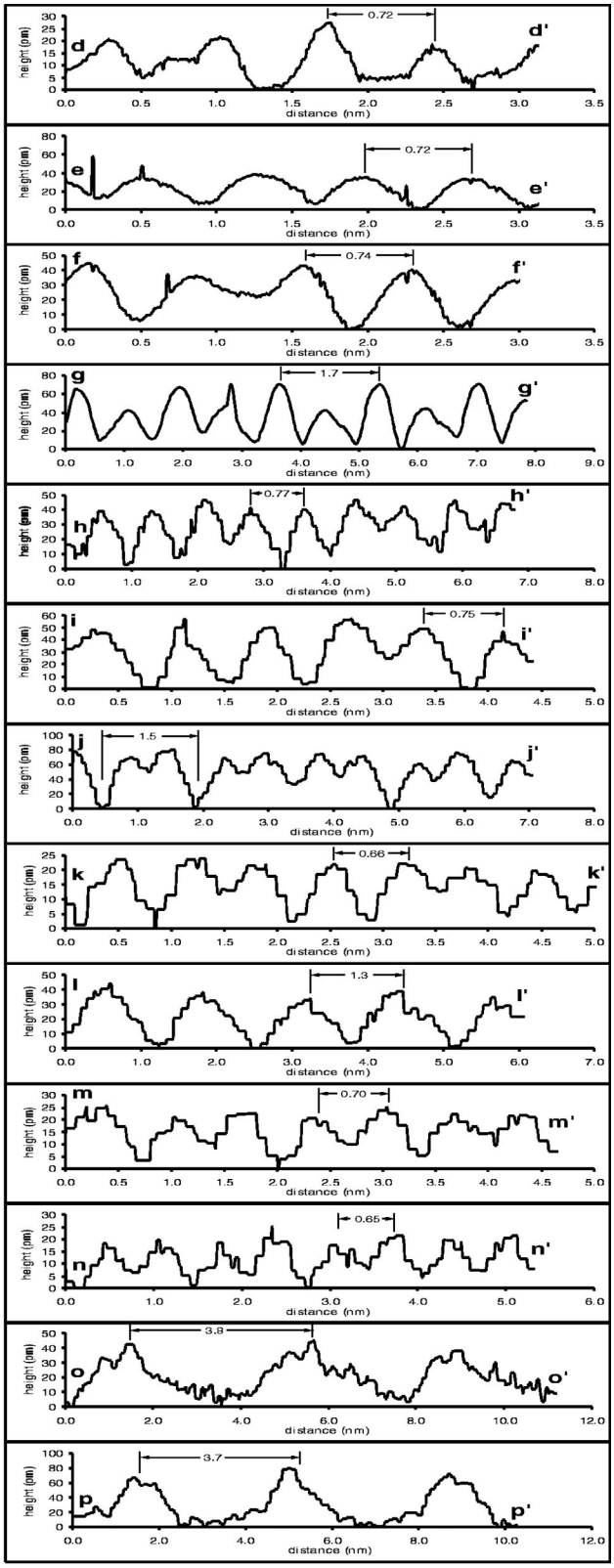

(d)

FIG. 5. STM images of tops of type-1 islands after annealing to (a) 800 °C ($V_T = 2.45$ V, 180 pA), (b) 900 °C ($V_T = 2.18$ V, 200 pA), (c) 1000 °C ($V_T = 1.0$ V, 340 pA), and (d) line profile cross sections indicated in images (a)–(c).

served sidewall rose at 60 ° from the substrate surface, but this could easily be limited by the shape of the STM tip and the true sidewall could be steeper.

While there was little change in the overall shape of type-1 islands with heat treatments (Fig. 1), the atomic-scale structure, observed by STM, of the flat tops of the islands, varied considerably with annealing temperature and scanning parameters (tip state and bias voltage). Figure 5(a) shows an STM image of one of these structures observed on the top of an island after annealing to 800 °C. Line profiles connecting the marked points are shown in Fig. 5(d). The structure is ordered with a period (along g-g') of 1.7 ± 0.2 nm and is composed of rows (d-d') with a period of 0.72 ± 0.05 nm. After heating to 900 °C, Fig. 5(b) was observed, again with 1D ordering with a period along the rows (h-h') and (i-i') of 0.77 ± 0.05 nm and 0.75 ± 0.05 nm, respectively. Across the rows the spacing alternates between large and small, with a period (j-j') of 1.5 ± 0.2 nm. As the (j-j') line is at an angle of 75° relative to the rows, the distance between rows is sin (75°) multiplied by 1.5 nm or 1.4 nm. Finally, after heating to 1000 °C the image shown in Fig. 5(c) was found. This structure also has a 1D ordered structure, but the row spacing (o-o') and (p-p') increased to 3.7 ± 0.2 nm and 3.8 ± 0.2 nm, respectively. Along the rows, the periodicity varied with location, with profiles (k-k'), (l-l'), and (m-m') having periods of 0.66 ± 0.05, 1.3 ± 0.2, and 0.7 ± 0.05 nm, respectively.

The structure observed after annealing to 1000 °C shown in Fig. 5(c), has what appears to be a tip-reconstruction event about one-third of the way down from the top of the image. As tunneling conditions can change with the reconstruction of the atoms on the tip of the STM, it is interesting to note the effect of the reconstruction on the imaging of the surface. The structure remains quite similar, but the corrugation (observed height variation) of the 3.7-nm period structure changes dramatically. Before the tip reconstruction, the corrugation along (o-o') is ~40 pm, and after the tip reconstruction, the corrugation along (p-p') is ~70 pm.

From examination of these observed structures and comparisons to the GIC literature,[16,12,17,15,13,14] we propose surface structures which reproduce the basic symmetries and periodicities observed on the type-1 islands. Figure 6(a) shows the region within the marked box in Fig. 5(b) (900 °C) enlarged and overlaid with 400 atoms of a Ni intercalant layer in graphite. The arrangement of overlaid Ni atoms is taken from the schematic shown in Fig. 6(b), drawn at the same scale. The locations of Ni atoms are marked with small black dots on white circles in the composite [Fig. 6(a)] and as black disks, drawn at the ionic bonding diameter of Ni in bulk (0.32 nm), in the schematic [Fig. 6(b)]. The structure has a nonprimitive, rectangular $\left|\begin{smallmatrix}3 & 0\\ -7 & 14\end{smallmatrix}\right|$ unit cell and a composition of NiC_{21}. [All unit cells described here are given in matrix notation and use unit vectors along the a_1 and a_2 directions marked in the lower-right corner of Fig. 6(b).] The composition stated corresponds to a single bilayer of Ni and graphite. The fit of the structure to the schematic model is superb, accurately reproducing both the periodicity and symmetry of the observed structure over a large scale. A primitive $\left|\begin{smallmatrix}3 & 0\\ -2 & 7\end{smallmatrix}\right|$ unit cell is also shown in the schematic [Fig. 6(b)] as it is more visually obvious than the orthogonal $\left|\begin{smallmatrix}3 & 0\\ -7 & 14\end{smallmatrix}\right|$ cell. The 75° angle of this nonorthogonal cell is marked in both the STM image and the schematic for comparison. It is also marked in the larger scale image, Fig. 5(b). Combined with the AES analysis of the islands that shows them to be composed of graphite and Ni, this structural match is convincing evidence of the formation of a Ni-GIC.

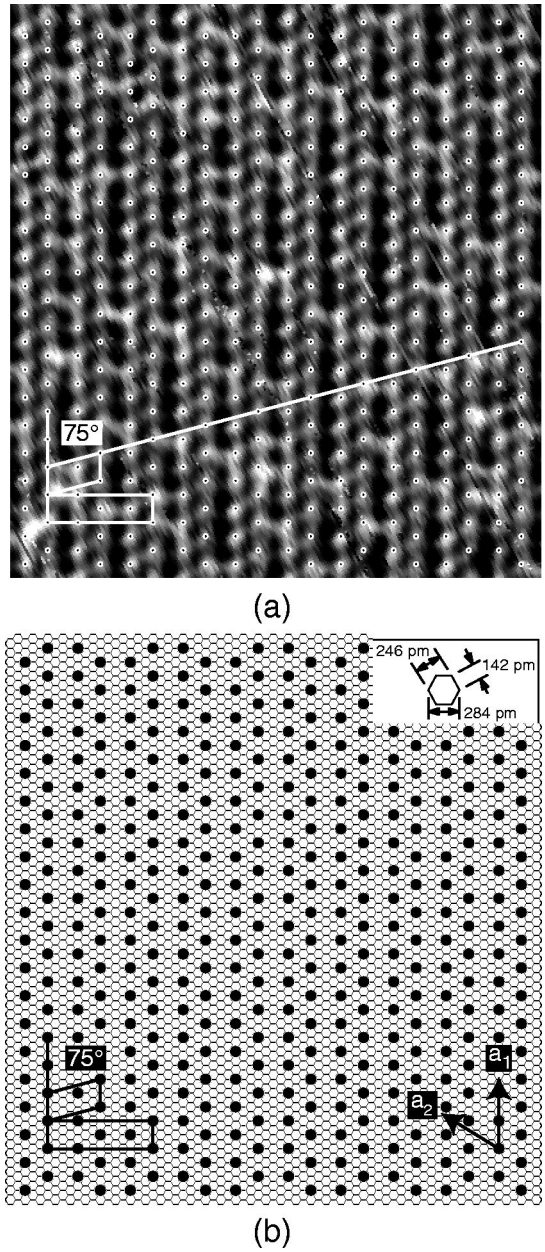

FIG. 6. (a) STM image from marked box in Fig. 5(b) (900 °C) with overlaid Ni-GIC lattice from (b). White circles around black dots are the locations of Ni atoms. (b) Schematic of the Ni-GIC lattice—solid disks are Ni atoms drawn at the ionic bond diameter of Ni in bulk (0.32 nm), and hexagons are graphite.

Deriving a structural model for the structures observed after annealing at 800 and 1000 °C was more problematic due to observed larger period one-dimensional oscillations.

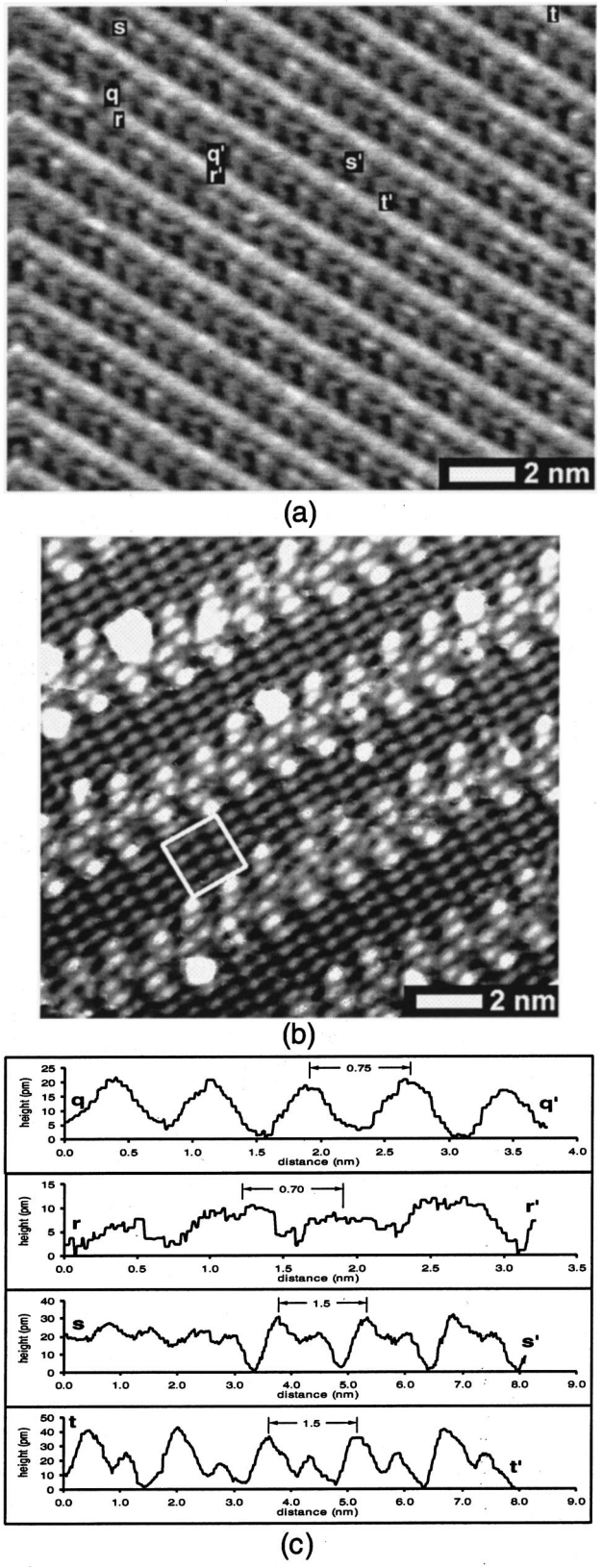

FIG. 7. STM images of type-1 islands after annealing to (a) 900 °C and (b) 1000 °C ($V_T = -2.0$ V, 250 pA) showing large period 1D corrugations. (d) line profile cross sections indicated in images (a), (b).

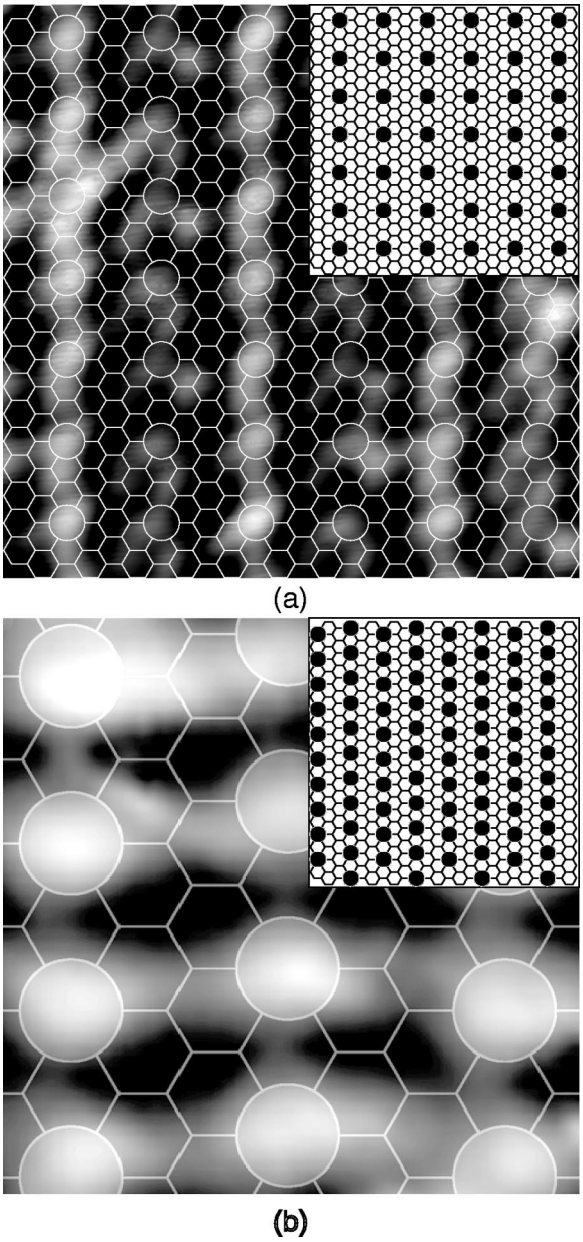

FIG. 8. Surface construction of Ni on graphite (a) at 800 °C from marked box in Fig. 5 and (b) at 1000 °C from marked box in Fig. 7(b). Insets are schematics of the proposed surface structures where solid circles are Ni atoms and hexagons are the underlying graphite.

These oscillations are briefly discussed above in reference to the tip reconstruction event in Fig. 5(c). The oscillations were observed at all temperatures and varied with tip potential and shape. Observations relating to this work are given below; however, a detailed explanation of these effects is left as a future study. Figures 7(a) and 7(b) show images observed after annealing to 900 and 1000 °C, respectively, and show this corrugation effect strongly. Figure 7(a), taken with another tip bias, appears to differ greatly from the other 900 °C scan [Fig. 5(b)], but examination of the line scans in Figs. 5(d) and 7(c) reveals that both 900 °C scans exhibit the same periodicities and symmetries. With the only systematic

difference between the two scans being the tip potential relative to the surface, we believe that this variation in observed corrugation arises from differences in the imaging of a surface graphite sheet. This result is similar to that observed by Olk *et al.*[18] where a $CuCl_2$ intercalant superstructure was imaged when the STM tip was positively biased with respect to the sample, and the overlying topmost graphite layer was imaged when the STM tip was negatively biased. The origin of the corrugation in the topmost graphite layer may be topographic (strain-induced buckling or subsurface ordering) or may be variation in electronic states, such as a charge density wave.[15–17]

While the corrugation of the topmost graphite makes it difficult to conclusively deduce intercalant lattice structures in the 800 and 1000 °C islands, examination of the symmetry and periodicity of the line profile sections given in Figs. 5(d) and 7(c) allows a reasonable hypothesis to be proposed. Figure 8(a) is an enlarged view of the marked box in Fig. 5(a) overlaid with a Ni intercalant structure for 800 °C. The inset is a schematic of the structure. The structure has a $\left|\begin{smallmatrix} 3 & 0 \\ -2 & 4 \end{smallmatrix}\right|$ unit cell and a composition of NiC_{24}. The match of this structure to the observed STM image is not as obvious as that shown in Fig. 6, but does accurately reproduce the observed periodicity and symmetry. The proposed 1000 °C structure, Fig. 8(b) has a $\left|\begin{smallmatrix} 2 & 0 \\ -3 & 6 \end{smallmatrix}\right|$ unit cell and a composition of NiC_{12}.

IV. CONCLUSIONS

When 2.5 ML nominal thickness Ni films were deposited onto single-crystal 6H-SiC (0001) substrates, at 600 °C, and subsequently annealed to 800–1000 °C, a new nickel graphite intercalation compound was observed. Studies with STM reveal islands of the Ni-GIC with flat tops exhibiting an ordered structure of Ni on graphite, and indexed patterns are proposed for three structures observed at 800, 900, and 1000 °C. This is the first known report of a Ni-graphite phase with significant C content and without residual constituents, such as chlorine, from a chemical intercalation process.

A second island type was also observed, and described, that formed when nickel silicide regions formed on the SiC substrate, then melted during high-temperature annealing. Comparisons to studies of bulk nickel silicides suggest that the NiSi phase formed, possibly stimulated by the Si-rich surface remaining after the growth of the described Ni-GIC. The formation of Si-rich nickel silicides has important technological implications for contact formation to SiC as it could result in a reduction in contact resistivity.

ACKNOWLEDGMENTS

This work was supported by Teknikvetenskapliga Forskningsrådet (TFR), Stiftelsen för Strategisk Forskning (SSF), the Swedish Institute, and the Natural Sciences and Engineering Research Council of Canada (NSERC).

*Present address: Department of Physics, Queen's University, Kingston, Ontario, Canada, K7L 3N6. Electronic address: robbie@physics.queensu.ca

[1] *Graphite Intercalation Compounds*, edited by H. Zabel and S. A. Solin (Springer-Verlag, Berlin, 1990), Vols. 1 and 2.

[2] V. F. Elesin and L. A. Openov, Surf. Sci. **442**, 131 (1999).

[3] V. K. Sharma and A. Baiker, Synth. Met. **11**, 1 (1985).

[4] I. S. Suzuki, E. C. Piscani, and M. Suzuki, Synth. Met. **73**, 55 (1995).

[5] X. Xu, N. Q. Wang, and Q. E. Zhang, J. Mol. Struct. **247**, 93 (1991).

[6] D. Guerard and V. A. Nalimova, in *Solid State Ionics*, edited by G. A. Nazri, J. M. Tarascon, and M. Schreiber, Mater. Res. Soc. Symp. Proc. No. **394** (Materials Research Society, Pittsburgh, 1995), p. 155.

[7] A. T. Shuvaev, B. Yu., Helmer, V. L. Kraizman, T. A. Lyubesnova, A. S. Mirmilstein, L. D. Kvacheva, Yu. N. Novikov, and M. E. Vol'pin, Physica B **158**, 539 (1989).

[8] H. Shioyama, H. Sakakihara, N. Iwashita, K. Tatsumi, and Y. Sawada, J. Mater. Sci. Lett. **13**, 1056 (1994).

[9] L. Grigorian, S. Fang, G. Sumanasekera, A. M. Rao, L. Schrader, and P. C. Eklund, Synth. Met. **87**, 211 (1997).

[10] G. V. Prudnikova, A. G. Vjatkin, A. V. Ermakov, A. M. Shikin, and V. K. Adamchuk, J. Electron Spectrosc. Relat. Phenom. **68**, 427 (1994).

[11] V. van Elsbergen, H. Nienhaus, and W. Monch, Mater. Sci. Forum **264–268**, 335 (1998).

[12] D. Anselmetti, R. Wiesendanger, and H. J. Guntherodt, Phys. Rev. B **39**, 11 135 (1989).

[13] D. Anselmetti, V. Geiser, G. Overney, R. Wiesendanger, and H.-J. Güntherodt, Phys. Rev. B **42**, 1848 (1990).

[14] D. Anselmetti, V. Geiser, D. Brodbeck, G. Overney, R. Wiesendanger, and H.-J. Güntherodt, Synth. Met. **38**, 157 (1990).

[15] H. P. Lang, R. Wiesendanger, V. Thommen-Geiser, and H. J. Güntherodt, Phys. Rev. B **45**, 1829 (1992).

[16] H. P. Lang, V. Thommen-Geiser, and R. Wiesendanger, Ultramicroscopy **42–44**, 624 (1992).

[17] K. Miyake, Y. Aiso, M. Komiyama, and H. Shigekawa, Scanning Microsc. **8**, 459 (1994).

[18] C. H. Olk, J. Heremans, M. S. Dresselhaus, J. S. Speck, and J. T. Nicholls, Phys. Rev. B **42**, 7524 (1990).

[19] S. P. Kelty and C. M. Lieber, J. Phys. Chem. **93**, 5983 (1989).

[20] C. Klink, L. Olesen, F. Besenbacher, I. Stensgaard, E. Lægsgaard, and N. D. Lang, Phys. Rev. Lett. **71**, 4350 (1993).

[21] S. Yamazaki, M. Tanaka, S. Tanaka, M. Fuginami, R. Uemori, D. Fujita, T. Homma, and M. Ono, J. Vac. Sci. Technol. B **9**, 883 (1991).

[22] C. Klink, I. Stensgaard, F. Besenbacher, and E. Lægsgaard, Surf. Sci. **342**, 250 (1995).

[23] G. Hörmandinger, J. B. Pendry, F. M. Leibsle, P. W. Murray, R. W. Joyner, and G. Thornton, Phys. Rev. B **48**, 8356 (1991).

[24] R. Koch, O. Haase, M. Borbonus, and K. H. Rieder, Phys. Rev. B **45**, 1525 (1992).

[25] M. F. Singelton and P. Nash, in *Binary Alloy Phase Diagrams*, edited by T. B. Massalski (American Society for Metals, Metals Park, OH, 1986), Vol. 1, p. 578; P. Nash and A. Nash, *ibid.*, Vol. 2, p. 1755.

[26] A. T. Shuvayev, B. Yu. Helmer, T. A. Lyubeznova, V. L. Kraiz-

man, A. S. Mirmilstein, L. D. Kvacheva, Yu. N. Novikov, and M. E. Volpin, J. Phys. (Paris) **50**, 1145 (1989).
[27] K. Robbie, S. T. Jemander, N. Lin, R. Erlandsson, G. V. Hansson, and L. D. Madsen, Mater. Sci. Forum **338–342**, 981 (2000).
[28] F. Owman and P. Mårtensson, Surf. Sci. **324**, 211 (1995).
[29] Cree Research Inc., Durham, NC, www.cree.com.
[30] C. Hallin, F. Owman, P. Mårtensson, A. Ellison, A. Konstantinov, O. Kordina, and E. Janzen, J. Cryst. Growth **181**, 241 (1997).
[31] F. Owman, C. Hallin, P. Mårtensson, and E. Janzen, J. Cryst. Growth **167**, 391 (1996).
[32] V. Ramachandran, M. F. Brady, A. R. Smith, R. M. Feenstra, and D. W. Greve, J. Electron. Mater. **27**, 308 (1998).
[33] Minolta Co., Ltd., Osaka, Japan, www.minolta.com.
[34] VG Scientific, West Sussex, UK, www.vgscientific.com.
[35] Digital Instruments, Santa Barbara, CA, www.di.com.
[36] Adobe Systems Inc., San Jose, CA, www.adobe.com.
[37] F. Owman and P. Mårtensson, J. Vac. Sci. Technol. B **14**, 933 (1996).
[38] T. Tsukamoto, M. Hirai, M. Kusaka, M. Iwami, T. Ozawa, T. Nagamura, and T. Nakata, Appl. Surf. Sci. **113/114**, 467 (1997).
[39] L. D. Madsen, E. B. Svedberg, H. H. Radamson, C. Hallin, B. Hjorvarsson, C. Cabral, J. L. Jordan-Sweet, and C. Lavoie, Mater. Sci. Forum **264–268**, 799 (1998).
[40] B. Pecz, G. Radnoczi, S. Cassette, C. Brylinski, C. Arnodo, and O. Noblanc, Diamond Relat. Mater. **6**, 1428 (1997).
[41] J. I. Goldstein, D. E. Newbury, P. Echlin, D. C. Joy, A. D. Romig, Jr., C. E. Lyman, C. Fiori, and E. Lifshin., *Scanning Electron Microscopy and X-Ray Microanalysis* (Plenum, New York, 1992).
[42] A. Amoddeo, L. S. Caputi, and E. Colavita, J. Electron Spectrosc. Relat. Phenom. **62**, 263 (1993).
[43] S. Ingrey, M. B. Johnson, R. W. Streater, and G. I. Sproule, J. Vac. Sci. Technol. **20**, 968 (1982).
[44] J. C. Schuster, Int. J. Refract. Met. Hard Met. **12**, 178 (1994).
[45] P. Villars, A. Prince, and H. Okamoto, *Handbook of Ternary Alloy Phase Diagrams* (American Society for Metals, Metals Park, OH, 1995), Vol. 6, p. 7236.